Lenslet VR: Thin, Flat and Wide-FOV Virtual Reality Display Using Fresnel Lens and Lenslet Array

Kiseung Bang, Youngjin Jo, Minseok Chae and Byoungho Lee, *Fellow, IEEE*

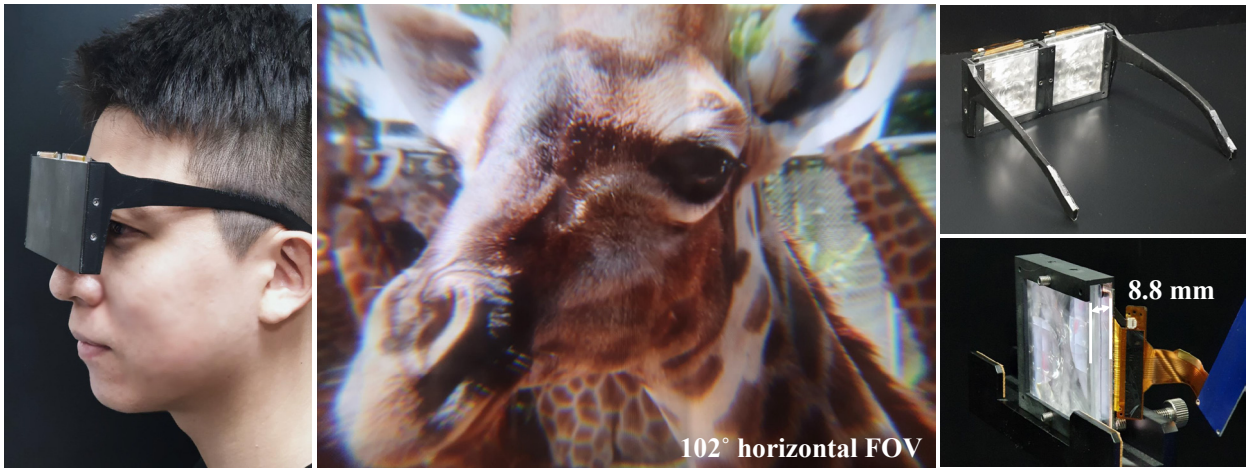

Fig. 1. (Left and right top) VR glasses prototype. (Right bottom) The monocular module of VR glasses prototype. The total thickness, including all optical components, required space, and the LCD is 8.8 mm. (Middle) Captured result of display experiment with the monocular benchtop prototype. The prototype covers a 102° x 102° FOV. The photo was taken with Samsung Galaxy S10 5G smartphone ultra-wide-angle camera (f/2.2, 1.8 mm), which has a 104° x 88° FOV. The photo is a single frame in a video. Captured video result is provided in supplementary media. Video by HDVMaster on Motion Elements.

Abstract—We propose a new thin and flat virtual reality (VR) display design using a Fresnel lenslet array, a Fresnel lens, and a polarization-based optical folding technique. The proposed optical system has a wide field of view (FOV) of 102°×102°, a wide eye-box of 8.8 mm, and an ergonomic eye-relief of 20 mm. Simultaneously, only 3.3 mm of physical distance is required between the display panel and the lens, so that the integrated VR display can have a compact form factor like sunglasses. Moreover, since all lenslet of the lenslet array is designed to operate under on-axis condition with low aberration, the discontinuous pupil swim distortion between the lenslets is hardly observed. In addition, all on-axis lenslets can be designed identically, reducing production cost, and even off-the-shelf Fresnel optics can be used. In this paper, we introduce how we design system parameters and analyze system performance. Finally, we demonstrate two prototypes and experimentally verify that the proposed VR display system has the expected performance while having a glasses-like form factor.

Index Terms—Virtual reality, Near-eye display, Lenslet array, Fresnel lens

1 Introduction

Virtual reality (VR) technology has attracted much attention because of its huge potential applications such as entertainment, education, training, fine arts, and social communication. However, although several decades have passed since the first commercialized product came out, VR has not yet reached the mainstream. VR fans who use VR for a long time in their daily life are still few. According to a survey of VR experts [17], the biggest hindrance in current VR is the discomfort due to heavy and bulky headset-type hardware rather than high price or insufficient content. However, ironically, it is *the empty space* that currently takes up most of the volume in commercial VR devices. This space is required by the optical design using a single floating lens for each eye. This primitive optical design has been used without drastic changes since the early days of VR. While many other VR technologies, such as real-time tracking and rendering, show the rapid growth, the development of optical system design has been stagnant. The slow development of optical design has been a bottleneck for the explosive expansion of VR. In order to widen this bottleneck and open a new page of the VR market, the next-level VR optics is required.

Recently, two important approaches have been proposed to make a compact VR display system. First, Ratcliff et al. proposed a VR display system with a 180° field of view (FOV) using a curved lenslet array [33]. Thanks to the short focal length of the lenslet array, their VR design requires a shorter distance to float the display image. In addition, the curvature of the lenslet array enlarges the FOV and creates an eyebox at an appropriate distance. However, their system requires a curved display and a lenslet array with an individually optimized lenslet, which is quite complicated to implement. Also, the prototype they demonstrated had a 40 mm thickness, which is still not small enough.

Second, Maimone and Wang proposed a flat VR display system using a polarization-based optical folding technique and a holographic lens [25]. They demonstrated a sunglasses-sized prototype with 9 mm thickness and 90° horizontal FOV thanks to the very low f-number

All authors are with School of Electrical and Computer Engineering, Seoul National University.

E-mail: kiseung.bang@gmail.com / niugnas@snu.ac.kr / mschae3d@gmail.com / byoungho@snu.ac.kr.

Manuscript received 9 Sept. 2020; revised 15 Dec. 2020; accepted 8 Jan. 2021. Date of publication 23 Mar. 2021; date of current version 7 Apr. 2021. Digital Object Identifier no. 10.1109/TVCG.2021.3067758

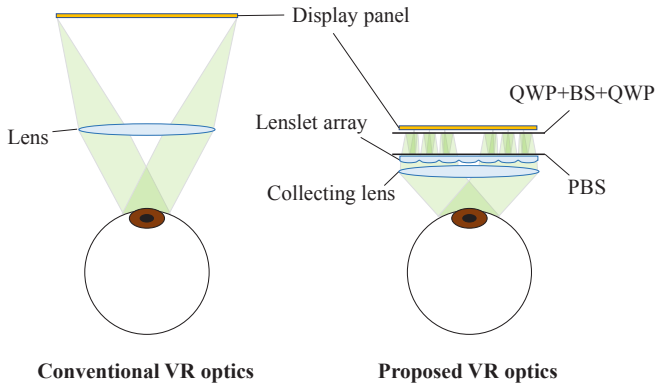

Fig. 2. (Left) Conventional VR optics using a floating lens. (Right) Proposed VR optics using a lenslet array and a collecting lens. Polaization-based optical folding technique is applied for further shortening the thickess. QWP: quarter wave plate, BS: beam splitter, PBS: Polarization beam splitter.

of the holographic lens and the folded path length. However, since holographic lenses in their systems are highly dispersive, complex systems such as R, G, B laser sources and multiplexed holographic lenses are required for full-color display. Also, holographic lenses have high angular selectivity, limiting the system's eye-box. Most importantly, the immature fabrication technology of the holographic lens is very detrimental to display uniformity.

We propose a new VR display design as an advanced combination of the above two approaches. The new VR design is composed of a Fresnel lenslet array and a Fresnel lens. In this system, we reduce the required space using both the lenslet array and the polarization-based optical folding technique. As a result, the proposed design requires only 3.3 mm of spacing. Simultaneously, due to the additional Fresnel lens, the proposed design has a wide field of view (FOV) of 102° x 102° and a wide eye-box of 8.8 mm, and an ergonomic eye-relief of 20 mm, while having a flat structure. Since all optical elements in this system operate in an on-axis condition, the proposed system can be made with off-the-shelf on-axis optics without additional optimizations. Moreover, the lenslet's on-axis operation provides a continuous pupil swim distortion within the eye-box.

In this paper, we introduce the overall principle of VR optical design. We clarify the problem of the conventional VR display; we start to design the proposed system as a solution to the problem. We derive a proper specification of the optical system, and finally, we demonstrate a glasses-sized wide-FOV, wide-eye-box, and full-color VR display prototype. The total thickness of our optical module, including the display panel, is 8.8 mm. If only the redundant thickness of commercial optical elements is reduced, it is possible to implement a 6.3 mm-thick system. Through the display experiments, we confirm that the prototype has excellent performance as designed.

1.1 Contributions

The contribution of our work is as follows:

- To the best of our knowledge, we first optimized a lenslet-array-based flat VR design even further considering FOV, eye-box, eye-relief, resolution and system thickness. Our novel VR design requires only 3.3 mm of a short physical distance inside the system while having a state-of-the-art level of FOV (102° x 102° for each eye), wide eye-box (8.8 mm x 8.8 mm), uniform color image and even suitable for mass production.
- The proposed VR optical system has a wider design space than the conventional VR design. We derived optical system parameters that simultaneously satisfy wide FOV, sufficient eyebox, proper eye-relief, and thin form factor.
- We analyzed the effect of the optical aberration of Fresnel optics on the image distortion and usable eye-box of the proposed system and confirmed it through experiments.
- We demonstrated the benchtop prototype and VR glass prototype and confirmed the feasibility of the proposed design.

2 Related Works

2.1 Conventional VR optics

Currently, most commercialized VR devices have conventional VR optics systems using a single lens per eye [19, 37]. The conventional system has a trade-off relationship between FOV and system size. Popular products usually have a binocular FOV of 90° to 110° and have a headset shape with a thickness of about 5 cm and a width of about 15 cm [2, 6]. On the other hand, there are also VR headset products that have a wide binocular FOV of 180° to 210°. It is advantageous in providing an immersive experience, but these have a large system size with a thickness of around 10 cm and a width of around 30 cm. [4, 5, 7]. Our proposed system can break the conventional trade-off between the form factor and the FOV and achieve both simultaneously, which is explained in Section 3.

2.2 Pancake VR optics

There are many studies to reduce the size of VR optical systems. Among them, the optical path folding technique, which is called a pancake lens, can make the system's optical path length longer than the physical distance [29, 42]. In the pancake lens system, light bounces back and forth between the curved surfaces with polarization-dependent coating, resulting in shortening the required physical distance. A recently demonstrated prototype showed a goggle-like form factor with a thickness of 3 to 4 cm [3]. Recently, Maimone and Wang applied the principle of a pancake lens to a flat VR system using a holographic lens. They demonstrated a sunglasses shaped prototype with a sub-centimeter thickness. Our proposed system is also a flat structure, so this method can be applied as it is, which is explained in detail in Section 3.4.

2.3 Lenslet array and light field near-eye display

The lenslet array can have a short focal length due to the small aperture of each lenslet. Many researchers have proposed a compact near-eye display using a lenslet array [10, 12, 15, 21, 22, 30, 35, 38, 40, 43–45]. However, many of the studies focused more on 3D display capability rather than display performance, and their systems did not have a sufficient FOV, resolution and a proper eye-relief. Recently, Ratcliff et al. demonstrated a 180° FOV prototype using a curved lenslet array [33]. They enlarged the FOV by forming an eye-box in the center of the curvature. The main idea of our proposed system is similar. However, we use an additional collecting lens instead of curvature. It has a similar effect of enlarging the FOV while having a flat and simple structure. Some researchers have proposed a light field near-eye display using a pinhole array instead of a lenslet array [8, 9, 16, 24]. It can implement a wide FOV system, but it has the disadvantages of pinpoint eye-box size and limited resolution due to pinhole diffraction.

2.4 Waveguide near-eye displays

Waveguide near-eye displays have been studied a lot for augmented reality (AR) display rather than VR display [11, 19, 23, 32, 36, 47]. It has a very thin form factor of 1 to 2 mm and provides a very wide eyebox due to an exit-pupil expanding effect. However, since an optical lens power cannot be provided in the waveguide display, it has only a limited FOV equal to the waveguide's angular bandwidth. Recent commercial products in the market have a diagonal FOV of 40 to 50 degrees, which is not sufficient for VR applications yet [1, 20].

3 Design Approach

3.1 Why conventional VR is bulky

Before introducing the new design, we clarify why the conventional VR systems have a large volume because the new design originated as a solution to the conventional system's fundamental problem.

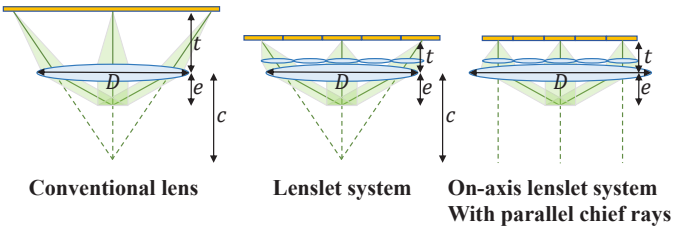

Fig. 3. Simplified optical structure layouts. (Left) Conventional VR optics. (Middle) Off-axis lenslet system (Right) On-axis lenslet system. Green solid lines are the chief rays or central chief rays.

A combination of the two reasons explains the cause of the problem. First, the conventional VR optical system is composed of a single lens, as shown in Fig. 2 (left), which has the role of floating the display panel to a long distance. Because of this role, the required optical system distance t between the lens and the display panel must be equal to the lens focal length f. (See Fig. 3 (left))

$$t = f. \tag{1}$$

Second, the lens also has the role of collecting light from the display panel to the user's eye. In other words, it forms an eye-box in which the user's eye should be placed to observe the image. For VR users' comfortable wearability, the eye-relief e, which is the distance from the last lens surface to the eye-box, should not be too short or too long. Approximately 20 mm is an ergonomically typical target. The eye-relief e is determined by the focal length f and the converging distance c of the chief rays from the lens.

$$1/e = 1/f + 1/c. \tag{2}$$

Since the eye-relief e has an ergonomically determined optimal value, for a shorter optical system distance t, which is equal to the focal length f by Eq. (1), it would be advantageous to have a negative value of c, which means diverging chief rays. However, due to the following FOV equation, it cannot be a practical solution. The FOV of the system is limited by the eye-relief e and the lens aperture D.

$$FOV < 2\tan^{-1}(D/2e) = 2\tan^{-1}\left(\frac{1}{2}(D/f + D/c)\right). \tag{3}$$

The right side of the equation is the result of the substitution of Eq. (2). Note that D/f in the right-hand side is the f-number of the lens. There is a practical limitation on the f-number of a single lens. In order to have a low f-number, the lens must be very thick and simultaneously have severe optical aberration. Therefore, if c has a negative value, the system will have a smaller FOV with the same lens. In other words, conventional VR design has an unavoidable trade-off relation that wider FOV causes a thicker system.

Most VR designers selected wide FOV rather than the thin system with converging chief rays and positive value c. In this case, the following equation is valid.

$$e < f = t. \tag{4}$$

Although this analysis has many assumptions and simplifications, Eq. (4) fully explains the fundamental reason why the conventional VR design has to be a thicker system than the eye-relief distance.

3.2 Lenslet array and collecting lens

3.2.1 Thinner system

The reason for the disadvantageous relationship between eye-relief and optical system distance in Eq. (4) is that both values are related to the focal length f of the lens in Eqs. (1) and (2). In other words, the conventional VR design is thick because the single lens performs two different functions at the same time:

1. To float the display panel at a far distance or infinity.
2. To collect the light from the display panel to the eye-box

We try to solve the problem by breaking the link between these two functions. Instead of a single lens, our proposed system consists of a lenslet array and a collecting lens, as shown in Fig. 3 (center). The display panel and the lenslet array are parallel to each other with an optical system distance of t, and the collecting lens is attached as close as possible to the lenslet array. The lenslet array is in charge of the first function, and the collecting lens is in charge of the second function. In this system, the optical system distance t and the eye-relief e are determined as follows.

$$1/t = 1/f_1 + 1/f_2, \tag{5}$$

$$1/e = 1/f_2 + 1/c, \tag{6}$$

where f_1 and f_2 are the focal lengths of the lenslet array and collecting lens, respectively. At this time, the displayed image should be divided into multiple areas corresponding to each lenslet. Here we define central chief rays as the rays passing through both the center of lenslets and the center of the eye-box. c is the converging distance of the central chief rays starting from the center of each divided area of the display panel. Looking at Eqs. (5) and (6), the number of system parameters we can control is no longer one (f), but two (f_1 and f_2), which is equal to the number of the system performance values t and e. In other words, in this proposed system, we can set the optical system distance t and eye-relief e independently without a trade-off relation. Therefore, the proposed system can have a much shorter optical system distance than the eye-relief.

3.2.2 Less aberration

We also want this system to be advantageous in terms of optical aberration. We present two simple comparisons. First, we can compare the conventional lens system and lenslet array system shown in Fig. (3) (left) and (middle). In general, a single optical lens shows its best imaging performance in the center. However, in the conventional lens system, since the light from a peripheral display pixel is incident on the lens's peripheral region, the imaging quality is lower than that of the center.

On the other hand, in the lenslet system, even light from a peripheral display pixel is incident at the corresponding lenslet's center. Also, each peripheral lenslet can be independently optimized to have the least aberration. In other words, there is a room for localized optimization. Therefore, the lenslet system can have less aberration in the peripheral sight than the conventional lens system. It is also necessary to consider the peripheral aberration of the collecting lens. However, note that if two systems have the same system distance, the focal length of the collecting lens in the lenslet system is longer and has less aberration.

Secondly, we compare two cases where the lenslet system has converging central chief rays and parallel central chief rays, as shown in Figs. 3(middle) and (right). In a converging system, each lenslet operates in off-axis conditions. Even if well optimized for the off-axis condition, the imaging quality in each lenslet's peripheral area will decrease dramatically compared to the lenslet center.

On the other hand, in the parallel system, since all lenslets operate in on-axis conditions, better image quality can be provided in each lenslet's peripheral region. Besides, since all on-axis lenslets are identical, unlike in the off-axis condition, it also has the advantage that it is not necessary to optimize each lenslet individually. Also, since many commercial lenses on the market are designed for the on-axis operation, we can utilize already developed resources. As a result, we selected the on-axis lenslet design with parallel central chief rays. In this case, c in Eq. (6) becomes infinity, and the following equation holds instead.

$$e = f_2. \tag{7}$$

3.3 Fresnel lens

Lenslet system reduces the required optical system distance in VR display system. However, to achieve a sunglasses size, each optical component must also be thin. Therefore, a conventional thick lens or lenslet array is not the right choice, especially when a low f-number is required for wide FOV. As a thin low f-number lens, we can consider a Fresnel lens, surface relief grating (SRG), volume hologram, etc. We compare the characteristics of these optical elements and select the proper one for the system.

First, SRG and volume hologram are classified as diffractive optical elements (DOEs) because they deflect light using diffraction. When the transmittance, refractive index, or surface shape of a substrate medium changes with a specific period, the diffraction angle θ_d is determined by the period Λ and the wavelength of light λ.

$$\theta_d = \sin^{-1}\left(\sin\theta_{in} + m\frac{\lambda}{\Lambda}\right), \tag{8}$$

where θ_{in} is the incident angle and m is an integer number. Since both SRG and volume hologram have no limit to the range of deflection angle and only need micrometer-level thickness, it is suitable for realizing a thin and low-f-number lens. However, since the diffraction angle is too highly dependent on the wavelength, DOE has highly dispersive optical properties (e.g., focal length). With a broad spectrum light source, it will have severe chromatic aberration. Therefore, for full-color display, at least three laser sources corresponding to R/G/B color must be used, and three DOEs responding to each wavelength must be multiplexed, which makes the system quite bulky and complicated.

Also, the diffraction efficiency of DOEs rapidly decreases as the incidence angle moves away from the designed central angle, which is called angular selectivity. The angular selectivity limits the DOE's numerical aperture (NA), resulting in limited eye-box size and uniform efficiency even within the limited size. Moreover, when the diffraction efficiency is lower than 100%, the light of the remaining energy passes through the DOE as if it is a glass plate, which may cause severe background noise in the VR display system.

On the other hand, Fresnel lenses have many advantages. Fresnel lenses deflect light using the refraction principle like a prism, so they are classified as refractive optical elements (ROEs). The Fresnel lenses have dense sawtooth-shaped prism arrays on the surface, which have optimized surface angles to deflect the incident light at the desired angle. When the light propagates from air into the prism array, the refraction angle θ_r is determined by the refractive index of the medium n, which is the Snell's law.

$$\theta_r = N(\theta_{in}) = \sin^{-1}\left(\frac{1}{n}\sin\theta_{in}\right). \tag{9}$$

The refraction is also dispersive because the refractive index of the medium n varies depending on the wavelength. However, the amount of variance in the visible range is relatively very small. Therefore, it has much less chromatic aberration compared to DOE, and the full-color display can be made with a single Fresnel lens and a broad spectrum display source.

Also, the efficiency of refraction is very high and uniform over almost all angular ranges. Therefore, a Fresnel lens has no NA limitation caused by a lack of efficiency, and it is possible to implement a display with uniform brightness. Besides, the Fresnel lens has an advantage in background noise because un-refracted light does not transmit through the surface. For the reasons listed above, we chose to use a Fresnel lenslet array and a Fresnel lens in this design.

3.4 Polarization-based optical folding (Pancake lens)

As briefly introduced in Section 2, the polarization-based optical folding technique, which is called a pancake lens, can be applied to our lenslet VR system [25]. This technique allows light to bounce back and forth between interfaces, making the effective optical path longer than the physical distance. It is very beneficial in reducing the thickness of VR devices. Using this, we can additionally reduce the physical system distance to be 1/3 of the required optical system distance.

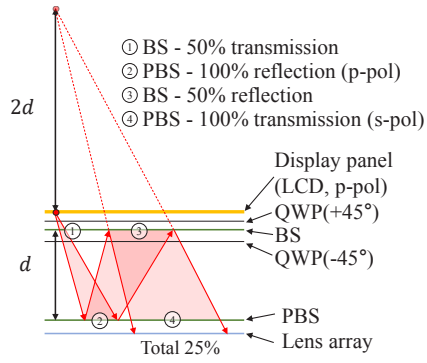

Fig. 4. The structure of polarization-based optical folding system. QWP: quarter wave plate, BS: beam splitter, PBS: polarization beam splitter

The structure of the pancake lens system is shown in Fig. 4. It consists of four additional planar surfaces: a quarter-wave plate (QWP), a beam splitter (BS), another QWP, and a polarization beam splitter (PBS) in order from the display panel to the lenslet array. First, the light emitted from a single pixel of the LCD panel is linearly-polarized. As this light passes through the QWP, BS, and another orthogonally aligned QWP, its polarization state is changed to the initial linear-polarization, and reflected by the PBS. After that, the light is reflected by the BS and then again incident on the PBS. In the meantime, the light passes through the single QWP twice and changes to the orthogonal linearly-polarized light. At this time, it passes through the PBS and propagates toward the lenslet array.

Since the light from the display panel repeatedly propagates between the BS surface and PBS surface three times, it is optically equivalent to the light from a farther distance by twice the distance between them. Since the QWP is very thin and the PBS and BS are closely attached to the LCD and the lenslet array, we can obtain an effective optical path three times longer than the physical system distance between the display panel and the lenslet array. That is, the physically required system distance can be reduced to 1/3 of the required optical system distance.

On the other hand, the pancake lens system has a disadvantage in terms of light efficiency. In the process of BS reflection and BS transmission, each 50% of light loss occurs. Therefore, the total light efficiency is theoretically only up to 25%.

4 Design Space

In this section, the specification of optical elements is selected so that the proposed system has a wide FOV, wide eye-box, ergonomic eye-relief, and thin form factor. In this section, we assume ideal lenses rather than practical Fresnel lenses for intuitive understanding. An analysis of the practical Fresnel lens is followed in Section 5.

4.1 Light field analysis

Unlike the conventional VR design, understanding the propagation of light in the proposed lenslet VR design is not straightforward. The main reason is that the exit pupil cannot be clearly defined. By definition, each lenslet's exit pupil is the aperture of each lenslet itself, but in a combined system, the problem becomes complex. The most appropriate way to explain this is to use the light field. In the light field analysis, a ray on a certain plane is expressed as a vector containing the 2-dimensional position and 2-dimensional direction. An optical system can be analyzed with the vector set of all rays. However, for simplicity, we only focus on a single dimension among two dimensions in the plane because both axes will have an identical light field due to our design's symmetry. So, we define the light field as an ordered pair (2-dimensional vector) of position x and angle θ.

When all the light field in a certain plane are known, we can calculate

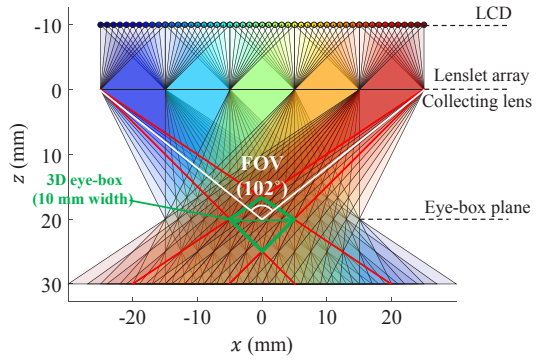

Fig. 5. The ray-tracing result of the proposed system. The light propagates from the LCD to the eye-box plane. The optical folding system and cross-talk between adjacent lenslets are omitted for simplicity. Lenslet array and collecting lens are assumed to have an ideal lens function. Each pixel of the LCD panel is distinguished by color, and so are the beams from each pixel.

the light field after the propagation by a distance of z as follows.

$$\begin{pmatrix} x' \\ \tan\theta' \end{pmatrix} = \begin{pmatrix} 1 & z \\ 0 & 1 \end{pmatrix} \begin{pmatrix} x \\ \tan\theta \end{pmatrix}. \tag{10}$$

And the light field right after passing through an ideal lens of focal length f is calculated by the following equation.

$$\begin{pmatrix} x' \\ \tan\theta' \end{pmatrix} = \begin{pmatrix} 1 & 0 \\ -1/f & 1 \end{pmatrix} \begin{pmatrix} x \\ \tan\theta \end{pmatrix}. \tag{11}$$

These two equations are all we need to analyze our system. Since $\tan\theta$ is used in both equations, in this paper we will use $(x, \tan\theta)$ instead of (x, θ) to express the light field.

Fig. 5 is the ray-tracing result in the proposed VR system. Each light originates from a single pixel on the LCD plane, and the light from each pixel is color-coded. We can derive the light field in each plane step by step from the LCD to the eye-box. First, Fig. 6(a) shows the light field in the LCD plane. The light field has a rectangular shape because it emits rays in all directions within the x range of the LCD size. Note that indicated by black lines are sets of light field originating from the sampled pixels. The light field after the propagation by the distance t is shown in Fig. 6(b). By Eq. (10), the rectangle is transformed into a parallelogram. However, we removed the light field incident on the adjacent lenslets from each LCD area. This is to remove the rays that cause cross-talk in advance. In other words, the cross-talk will be observed beyond this light field area. After that, the light field after passing through the lenslet array and collecting lens can be calculated as shown in Figs. 6(c) and (d) using Eq. (11). Finally, after the propagation by eye-relief distance e, the light field in the eye-box plane is calculated as shown in Fig. 6(e).

The result in Fig. 6(e) provides some good intuitions of the system. First, the result shows the parallelogram of light field that can be observed without the cross-talk. Suppose that the user's pupil is at x_0 in x-axis. Then, the corresponding vertical line in the light field is $x = x_0$. In order not to include cross-talk on the vertical line, x_0 must exist within the range indicated by the green double-sided arrow, which becomes the eye-box. The usable light field within this eye-box is marked with a green parallelogram. The vertical height of the parallelogram becomes the FOV. The range of FOV varies depending on the pupil position x_0, but the size remains the same in a tangential manner. Besides, the resultant black lines from each pixel become horizontal lines, which means the light becomes plane beam from the infinite focus distance at the eye-box. Note that multiple black lines from each pixel are combined to form a single black line within the available light field area,

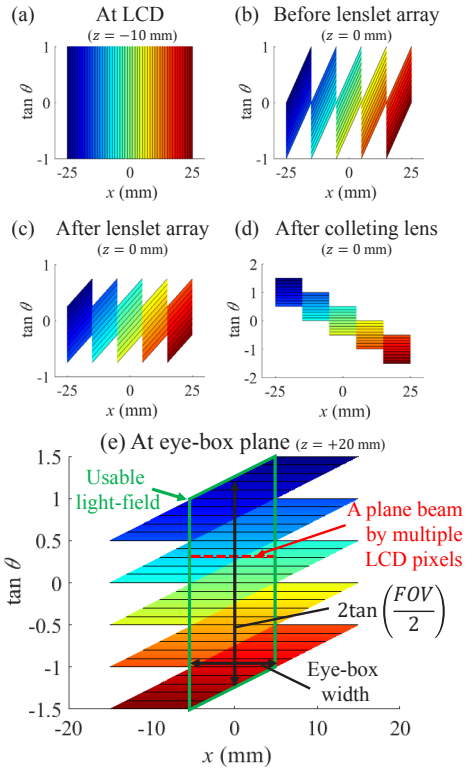

Fig. 6. The two-dimensional light field simulation results on each plane. The horizontal axis represents the position of rays, and the vertical axis represents the tangent value of the angle of rays. The light field originating from a single pixel of the LCD has the same color. To further emphasize this, the light field of the sampled pixels in a regular interval is marked in black.

as highlighted by a red dotted line. It means that several LCD pixels are used together to form one VR pixel. In other words, this system can deliver only a smaller number of VR pixels than the number of LCD pixels. In Section 4.2, we determine the specific system specification using this result.

4.2 Design parameter selection

The variables we can determine in this system are the focal length of the lenslet array f_1, the pitch of each lenslet p, the number of lenslets N (along a single axis), and the focal length of the collecting lens f_2. However, f_2 should be equal to eye-relief by Eq. (7). We selected $f_2 = e = 20$ mm. The objective functions of the system performance are eye-box EB, optical system distance t, and LCD resolution utilization rate R (along single axis). These are expressed as follows.

$$EB = f_2 p / f_1, \tag{12}$$

$$t = 1/(1/f_1 + 1/f_2), \tag{13}$$

$$R = f_1/(f_1 + f_2), \tag{14}$$

$$FOV = 2\tan^{-1}(Np/2f_2). \tag{15}$$

Among these, the eye-box, physical system distance, and LCD resolution utilization rate are plotted as a function of f_1 and f_2 in Fig. 7. Here, the physical system distance is calculated as $t/3$, considering the reduction using the optical path folding technique. We set the target LCD resolution utilization rate to 50% and the target eye-box to 10 mm. A red dotted line indicates these two conditions in Fig. 7. The shortest

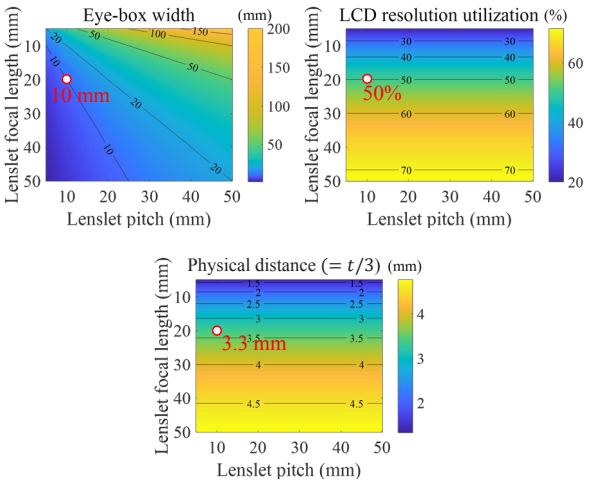

Fig. 7. Design space of the proposed system.

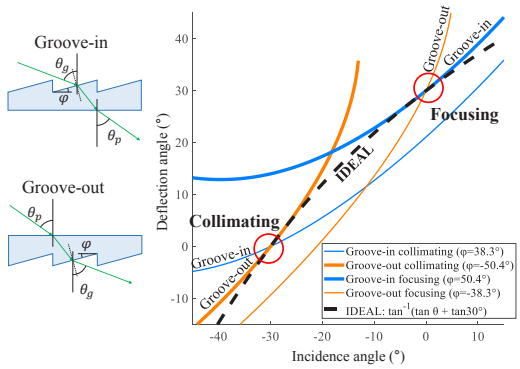

Fig. 8. (Left) Cross-section of a groove-in Fresnel lens and a groove-out Fresnel lens. (Right) The graph of the deflection angle according to the incidence angle in a groove-in Fresnel lens and a groove-out Fresnel lens. Marked as focusing means that the lens is designed to deflect the normal incident light (0°) to +30°, and collimating means −30° to the normal angle (0°).

physical system distance $t/3$ while achieving these targets is 3.3 mm at the circled condition where f_1 is 20 mm, p = 10 mm.

Looking at Eq. (15), FOV alone is a function of N. Therefore, the number of lenslets, N and FOV have no trade-off relation nor limitation. However, it may be difficult to secure an appropriate interpupillary distance (IPD) if the total width of the lenslet array is too wide. Considering the average IPD of 63 mm, we set $N = 5$ so that the total width of the lenslet array is 50 mm. Then, the FOV is 102.7°.

In this section, we assumed an ideal lens and lenslet array, so in many ways it will differ from the actual system. If the aberration of the actual Fresnel lens is considered, there will be more restrictions on the eye-box. This further analysis is continued in following section.

5 Aberration Analysis

Unfortunately, we could not find a perfect lens with a thin structure, as assumed in Section 4. Instead, we analyze the aberration of the system using Fresnel lenses. The aberration of the Fresnel lens will distort the system's light field, which may affect the system's FOV and eye-box. In this section, we determine the Fresnel lens structure and analyze the distortion.

5.1 Fresnel lens selection

Fresnel lenses can be thought of as a collection of fine prism pieces arranged on a plane. The optical properties of a Fresnel lens depend on many factors: the refractive index of the medium of the Fresnel lens, the surface angle of each prism piece, the angle of the sidewall, the groove density, the height of each prism and so on [13]. Here, the sidewall means the angle of the surface connecting two adjacent prism surfaces. However, if we assume that we are using a very thin and flat Fresnel lens with a very dense groove, which is quite correct in the experiment, the effect of other factors is negligible, and only the refractive index and surface angle of the medium matters. In this assumption, a deflected ray starts at the same position as the incident position without spatial shift inside the Fresnel lens. Therefore, we only focus on the angle of the deflection.

Fig. 8 (Left) shows the cross-sections of Fresnel lenses. Depending on whether the light is designed to be incident on the grooved face or the planar face, they are called groove-in and groove-out Fresnel lenses, respectively. In a groove-in Fresnel lens, the relationship between the incidence angle on the grooved face θ_g and the deflection angle on the planar face θ_p is calculated as the following equation with the Snell's law function $N(\theta)$ in Eq. (9).

$$\theta_p = N^{-1}(N(\theta_g - \phi) + \phi). \tag{16}$$

Here, ϕ is the surface angle of the prism piece at the incidence position. On the other hand, in a groove-out Fresnel lens, the incidence angle is θ_p, the deflection angle is θ_g, and by reciprocity, it becomes the inverse function of Eq. (16).

$$\theta_g = N^{-1}(N(\theta_p) - \phi) + \phi. \tag{17}$$

We have to decide whether to design the lenslet array and collecting lens in a groove-in type or a groove-out type. In the proposed design, the lenslet array should mainly collimate the light emitted from the LCD pixel, and the collecting lens should focus the parallel central chief rays toward the eye. Therefore, we compare which structure is more suitable for collimating and focusing, respectively.

For example, within a focusing lens, suppose that a normal incident ray should be deflected to +30° at a certain local position. The surface angle ϕ required for each groove-in and groove-out cases can be calculated by solving Eqs. (16) and (17). In each case, the deflection angle according to the incidence angle is plotted as a bold blue curve and an orange curve in Fig. 8 (Left). The black dashed line is the deflection angle in an ideal lens designed for the same purpose. Near the normal incidence, the groove-in Fresnel lens operates more similar to the ideal lens. That is, the focusing lens has much less aberration when designed in a groove-in Fresnel lens structure. Similarly, we can assume that the incidence ray at -30° should be deflected to the normal direction in a certain local position in a collimating lens. Then we can see that the collimating lens has less aberration when designed in the groove-out structure. Therefore, we decided to construct the prototype system using a groove-out collimating Fresnel lenslet array and a groove-in focusing Fresnel lens, as shown in Fig. 9. Note that both off-the-shelf products are readily available in the market.

5.2 Image distortion

Fig. 10 shows the light field in the eye-box plane, considering the actual Fresnel lenses' optical properties. Compared to the light field in the ideal lens system in Fig. 6(e), it is significantly distorted overall. However, there is no significant difference in the usable light field area indicated by the green parallelogram. It has the same 102° FOV as the ideal case and 8.8 mm eye-box width, which is only 12% less than the ideal case. It is because the distortion near the eye-box center is minimal, even when Fresnel lenses are used.

We can see the reason for low distortion by backtraced rays from the eye-box center, indicated by red lines in Fig. 9. First, since the focusing Fresnel lens is designed to change the on-axis parallel beam into the on-axis converging beam focused on the eye-box center, by reciprocity, it changes the backtraced rays to perfectly parallel rays. Also, since each collimating Fresnel lenslet is designed to change the on-axis diverging beam into the on-axis parallel beam, the backtraced parallel rays eventually converge to points at each lenslet's focal length. Note

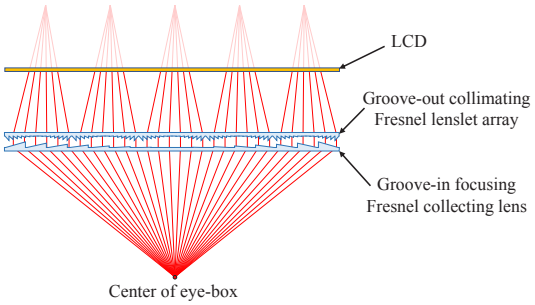

Fig. 9. The optimized Fresnel lens structure of the proposed design. The optical folding is omitted, and the gap between the lenslet array and the collecting lens is drawn exaggeratively large for intuitive visualization. The red lines are the reversely traced rays from the center of the eye-box to the LCD. Since both the lenslet array and the collecting lens are designed to have a planar beam on the grooved face, the traced rays have no distortion and are well focused on each virtual focal spot.

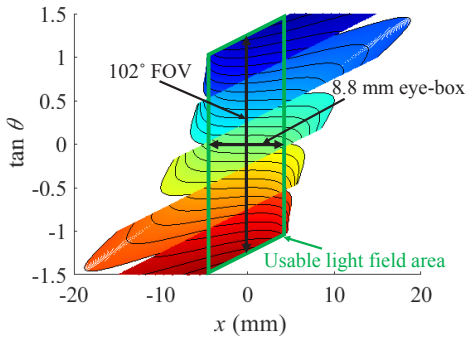

Fig. 10. Two-dimensional light field simulation results in the eye-box plane. The aberration of the Fresnel lens is considered in the calculation.

that despite the use of off-the-shelf optical elements, there is no aberration in all of these processes because each optical element operates under the designed conditions. When the pupil is at the center of the eyebox, the user will observe the image section where the backtraced rays meet the display panel plane. In other words, the user can observe the zero-distortion image without a specially optimized pre-distortion.

6 Implementation

6.1 Benchtop prototype

We demonstrate two kinds of prototypes. The first is the benchtop prototype shown in Fig. 11. This setup consists of an LCD, a Fresnel lenslet array, and a Fresnel lens. The LCD panel (Sharp, LS029B3SX02) has a 1440 × 1440 resolution, 36 μm pixel pitch and a thickness of 1.4 mm. As designed in Section 4, the Fresnel lenslet array (Fresnel Technologies, Inc.) has a 10 mm lenslet pitch and a 20 mm focal length. The Fresnel lens (Edmund Optics, 13-457) has a 20 mm focal length. Both Fresnel optics are made of an acrylic substrate and are designed to have a plane wave in the grooved face direction and a spherical wave in the planar face direction, as designed in Section 5. The Fresnel lenslet array and Fresnel lens have regularly spaced grooves, and the groove density for each is 80 grooves/cm and 98 grooves/cm. The thickness of each is 1.8 mm and 2.0 mm, respectively. Both were cut to 60 mm × 60 mm, while the actively used area was 50 mm × 50 mm. The Fresnel lenslet array and the Fresnel lens are attached closely with the grooved faces inside. The Fresnel optics is positioned 10 mm away from the LCD.

The image displayed on the LCD is calculated in a very simple way. As explained in Section 5.2, the proposed system can provide a distortion-free image, so there is no need for a complicated calculation

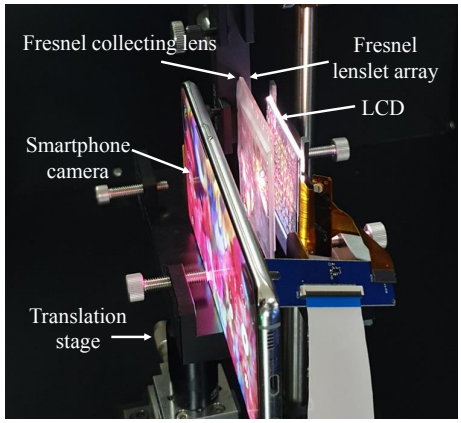

Fig. 11. The benchtop prototype consists of an LCD, a Fresnel lenslet array, and a Fresnel collecting lens. The optical folding system was not included.

process such as ray-tracing. We only need to crop and paste the corresponding part of the target image into each display area divided by the lenslet size. Therefore, the converting algorithm from a target image to the image to be displayed can be processed in real-time operation.

6.2 VR glasses prototype

Secondly, we demonstrated the VR glasses prototype. This setup includes a polarization-based optical folding system, in addition to the same LCD, Fresnel lens, and Fresnel lenslet array used in the benchtop prototype. The optical folding system includes a BS plate and 2 QWP films, wire grid film as a PBS. Here, the wire grid film was attached to an additional 0.5-mm-thick glass plate to maintain a flat structure, and a spacer was used to make the gap between BS and PBS. All optical elements were cut to have a size of 6 cm x 6 cm. As shown in Fig. 1 (Right bottom), we made a monocular VR module by fixing the LCD, spacer, and optical elements in a holder we made. Finally, we made the VR glasses prototype by connecting two identical modules, as shown in Fig. 1 (Right top). The thickness of the QWP films and the wire grid film is 80 μm. The thickness of the spacer is 1.8 mm. The system's total thickness from the backplane of the LCD to the front plane of the Fresnel lens was measured to be 8.8 mm.

Considering the folded optical path and the refractive index n, the total effective optical path t from the LCD plane to the Fresnel lenslet array's grooved face is calculated as follows.

$$t = 3t_{spacer} + (3t_{glass} + 4t_{QWP} + 3t_{BS} + t_{PBS} + t_{lenslet})/n. \quad (18)$$

Here, t_{spacer}, t_{glass}, t_{QWP}, t_{BS}, t_{PBS}, and $t_{lenslet}$ mean the thickness of the spacer, glass plate, QWP film, BS plate, wire grid film, and Fresnel lenslet array, respectively, and all media were assumed to have a refractive index $n = 1.5$. The result of addition coincides with the designed value of 10 mm.

7 Display Result

In this section, we experimentally confirm that the proposed system shows good performance consistent with the analysis.

7.1 Camera

In order to capture the same sight as the VR user will see, the camera must have a wide FOV of more than 100 degrees, and the entrance pupil must not be located too deep from the lens surface. For example, a fisheye lens has a very wide FOV, but its too deeply located entrance pupil cannot be located at the short eye-relief distance, resulting in a severe vignetting problem due to pupil mismatch. So, we used an ultra-wide-angle camera of Samsung Galaxy S10 5G smartphone, which has f/2.2, 1.8 mm focal length, 1.0 um pixel pitch, and 4608 × 3456 resolution. The FOV of the camera is 104.0° × 87.7° and confirmed

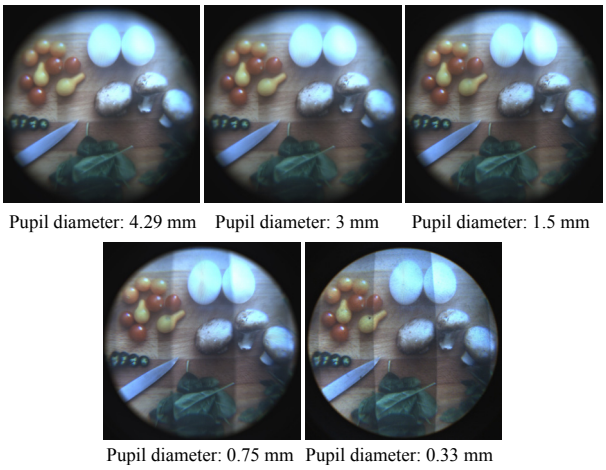

Fig. 12. Display results according to the pupil diameter (aperture size of the camera) with the benchtop prototype. The seam of the lenslet is quite indistinguishable, with the typical human pupil size of 2 mm to 8 mm. The results are captured with a camera lens of f/1.4, 2, 4, 8, and 16 and the focal length of 6 mm. Photo by Katie Smith on Unsplash.

with the test experiment result provided in the supplementary document. Except for Figs. 12 and supplementary image 7, all photos in this paper are captured with the camera and are in the original size, not cropped, so cover the maximum FOV of the camera.

7.2 FOV and image distortion

Fig. 1 (Middle) is the captured display result of the benchtop prototype. The camera is located at the center of the eye-box. The eye-relief was measured to be 20 mm. In the experimental results, the observed image almost perfectly fills the camera's maximum horizontal FOV of 104°, which matches well with the expected value of 102° FOV in the design. The vertical FOV of the camera is too narrow to cover this, but the vertical FOV of the prototype will be the same as the horizontal FOV due to the system symmetry. The captured image shows a clear and uniform color expression. In addition, all image pieces are continuously matched with each other at all edges between adjacent lenslets, so that they form one target image. However, the seam between the lenslets is observed as slightly darker lines than the surroundings, which was not predicted in simulation. This phenomenon occurs due to the physical seam at the junction between the lenslets. The physical seam is located very close to the eye. Therefore if the observer's pupil becomes larger, the seam image blurs more, then the user may not recognize it. The experimental result in Fig. 12 can verify it. The results show the captured images according to the camera aperture size. As the aperture diameter becomes larger than 3 mm, the seam becomes not so distinguishable. Although the photos in this paper taken by the smartphone camera with an aperture of 0.82 mm contain a noticeable seam, the seam will not be easily visible when observed by a human eye with a pupil diameter of 2 mm to 8 mm.

7.3 Eye-box and pupil swim distortion

Fig. 13 is the result of the pupil swim experiment with the benchtop prototype. As expected in the light field analysis in Section. 5.2, the cross-talk is observed only when the pupil position is further than 4.4 mm. Note that even when the whole observed image is distorted during the pupil swim, mismatch or discontinuity of image between adjacent lenslets is hardly observed. It means that the pupil swim distortion is mostly caused by the collecting lens, not the lenslet array. The captured images and grids at other sampled pupil positions are provided in the supplementary document. The eye-box range of 8.8 mm corresponds to the case where an eyeball with a rotation radius of 13 mm rotates by ±18.7°, that is, in a range of 37.4°, which is sufficient to cover a static VR experience [34].

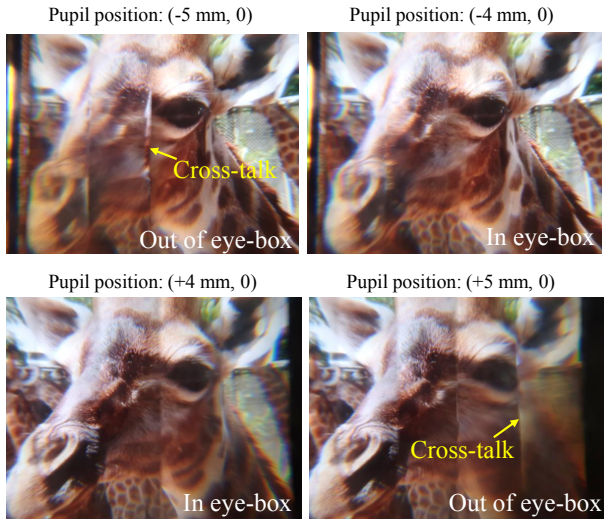

Fig. 13. Display results of pupil swim experiment in the benchtop prototype. The camera movement is along the horizontal axis. The cross-talk is detected when the pupil position is ±5 mm, not until ±4 mm. White arrows indicate the cross-talk.

7.4 Resolution and chromatic aberration

Fig. 14 is the result of capturing the resolution target image on the benchtop prototype. At the center of the sight, the finest line pair is resolved, which is corresponding to 4.8 ppd (pixels per degree). As the angular position goes further from the center, the resolution decreases. At 26.6°, the line pair with the period of 3 LCD pixels is resolved, which is 3.2 ppd. Similarly, at 45°, the system provides 2.4 ppd as the 4-pixel period line pair is resolved. Also, we have measured the modulation transfer function (MTF) which can also state the resolution of the optical system. MTF result can be found in the supplementary document [26].

In lower figures in Fig. 14, we can observe the chromatic aberration, which is low at the center and increases at the periphery. However, since the area where low aberration is observed is located very far from the center of the sight, it cannot be detected by the user's retinal fovea in general. Therefore, user inconvenience due to this reduction in resolution will be limited. In addition, the aberration of the proposed system is not so severe compared to current commercial VR products, so it will not provide extra discomfort to users.

7.5 VR glasses prototype

Fig. 15 shows the display result in the VR glasses prototype. Except for the addition of the optical path folding system, it is optically equivalent to the benchtop prototype, so there will be no differences in FOV, eye-box, distortion, resolution, etc. This is also confirmed in the experimental results. However, compared to the benchtop prototype, the display result of the VR glasses prototype contains blurry background noise. This is due to the blurred twin image created by unintentionally transmitted or reflected light from several additional internal surfaces. In the high contrast display results in the supplementary document, multiple twin noises due to pancake lens systems can be more clearly distinguished.

8 Discussion and Future Works

8.1 System thickness

In fact, the thickness of the off-the-shelf Fresnel lens and Fresnel lenslet array we used is quite thick. If thinner elements were used, the total thickness of the system could be further reduced. Assuming that both Fresnel lens and the Fresnel lenslet array are 0.5 mm thick, the spacer's

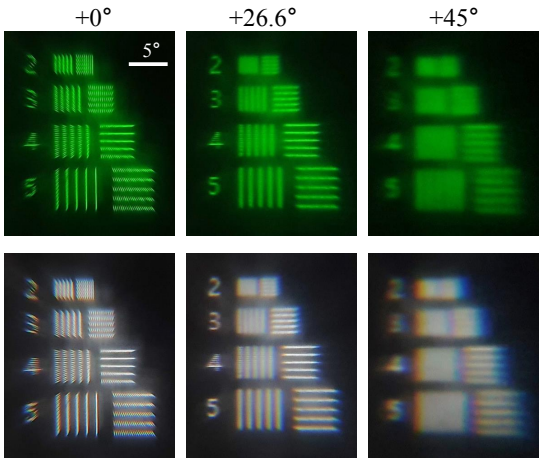

Fig. 14. The result of the resolution experiment in the benchtop prototype. Every line has one-LCD-pixel line width, and the periods of the line pairs are 2,3,4, and 5 pixels in order from the top. The same image was captured twice only with the color change between green mono and white. We can separately observe the chromatic aberration and image aberration. Each result is cropped from a wide-FOV image, which is provided in the supplementary document. The angles on the top indicate the horizontal angular position of the cropped image center.

Fig. 15. The display result of VR glasses prototype. The camera is located at the center of the eye-box. The photo is a screenshot of a video, which is provided in supplementary media.

thickness to satisfy Eq. (18) becomes 2.2 mm, and the total thickness can be reduced to 6.3 mm.

8.2 Leakage noise

The reason for the blurry background noise observed in the VR glasses prototype is the undesired reflection and transmission in multiple layers of the pancake lens system. There are two main reasons for this. First, the performance of the polarizing element is imperfect. The wire grid film (TECHSPEC) we used has a finite contrast ratio of 250:1. And the QWP (WP140HE polymer film) is designed to be used in 400-700 nm broad-spectrum but has a retardation error even within that range. For example, the wave retardation at 600 nm is about 0.235, not 0.25. Besides, noise may occur even when the polarization-dependent elements' fast axes directions do not perfectly match each other. If the polarization state can be controlled very precisely, noise can be significantly reduced.

The second reason is the surface reflection at the boundaries. This problem can be solved through the anti-reflection coating. The glass plate used in the experiment is not coated. BS plate has a broad-band anti-reflection coating, but it is designed for 45° incidence angle, so performance in the on-axis condition cannot be guaranteed. In our design, wide-angle broad-band anti-reflection coating is required because there is light in the range from $-45°$ to $+45°$ [31].

8.3 Fresnel lens optimization

System aberration, such as resolution decrease at the periphery and pupil swim distortion, is all due to the Fresnel lenses' aberration. If the Fresnel lens has less aberration through optimization, system performance can be improved. However, there is no left degree of freedom in the flat Fresnel lens structure that can be used for optimization other than the surface angle. So additional modifications such as a curved substrate or bi-convex Fresnel lens will be required [41]. Here, as stated in section 7.3, since the collecting lens affects the aberration and the pupil swim distortion much more than the lenslet array, the aberration optimization of the collecting lens may be more effective. Chromatic aberration due to dispersion, as well as imaging aberration, may be compensated through optimization [39, 46].

8.4 Pupil tracker synchronization

In the proposed system, two conditions limit the eye-box size. First, cross-talk by neighboring lenslets should not be visible. Second, image distortion should not be too severe. We can overcome the first limitation if we detect the pupil position in real time and change the displayed image corresponding to the position. Otherwise, we can physically move the optical system so that the pupil can keep inside the dynamic eye-box [18]. This method can solve the both cross-talk and distortion problems. In both methods, the user will see the image stably even if the pupil tracker does not have high accuracy as long as the pupil remains in the 8.8 mm wide eye-box.

8.5 See-through display

The proposed system is a VR display, but a compact wide FOV see-through augmented reality (AR) display can be made using the same principle. For that, a transparent display is required, and light from the outside and light from the display must be separated into different channels. We can try to utilize transparent screens such as holographic screens, and polarization-dependent optics such as anisotropic Fresnel lenses [14] or Pancharatnam-Berry phase lenses [27, 28].

9 Conclusion

Many people imagine the bright future of VR. As the technology advances, the number of VR users will increase, the field using VR will also expand, and sometime VR will be a part of daily life. However, such a future is possible only if a comfortable and long-time-wearable VR hardware becomes affordable to the public. In this paper, we proposed a possible solution of compact VR by optimizing the lenslet-array-based VR design to achieve a practical performance. Our proposed design can have sub-centimeter thickness, while having 102° monocular FOV which is comparable to current state-of-the-art VR products. It also has a stable eye-box and low pupil swim distortion. It delivers great color and can be combined with any display panel without spectrum limitation. At last, we already know how to mass-produce the necessary optical components for the Lenslet VR design. Maybe a daily VR is not that far away. We hope that our work can make an important contribution to expanding the world of VR.

Acknowledgments

This work was supported by Institute of Information & Communications Technology Planning & Evaluation(IITP) grant funded by the Korean government(MSIT) (No. 2017-0-00787)

REFERENCES

[1] Magic leap. https://www.magicleap.com/. Accessed: 2020-09-01.

[2] Oculus quest. https://www.oculus.com/quest/. Accessed: 2020-09-01.

[3] Panasonic vr eyeglasses. https://news.panasonic.com/global/press/data/2020/01/en200107-5/en200107-5.html. Accessed: 2020-09-01.

[4] Pimax 8k x. https://www.pimax.com/products/vision-8k-x. Accessed: 2020-09-01.

[5] Starvr. https://www.starvr.com/. Accessed: 2020-09-01.

[6] Vibe cosmos. https://www.vive.com/. Accessed: 2020-09-01.

[7] Xtal. https://vrgineers.com/. Accessed: 2020-09-01.

[8] K. Akşit, J. Kautz, and D. Luebke. Slim near-eye display using pinhole aperture arrays. *Appl. Opt.*, 54(11):3422–3427, Apr 2015.

[9] K. Akşit, J. Kautz, and D. Luebke. Slim near-eye display using pinhole aperture arrays. *Applied optics*, 54(11):3422–3427, 2015.

[10] R. Burke and L. Brickson. Focus cue enabled head-mounted display via microlens array. *TOG*, 32:220, 2013.

[11] D. Cheng, Y. Wang, C. Xu, W. Song, and G. Jin. Design of an ultra-thin near-eye display with geometrical waveguide and freeform optics. *Opt. Express*, 22(17):20705–20719, Aug 2014.

[12] P.-Y. Chou, J.-Y. Wu, S.-H. Huang, C.-P. Wang, Z. Qin, C.-T. Huang, P.-Y. Hsieh, H.-H. Lee, T.-H. Lin, and Y.-P. Huang. Hybrid light field head-mounted display using time-multiplexed liquid crystal lens array for resolution enhancement. *Optics Express*, 27(2):1164–1177, 2019.

[13] T. Fujii, A. Goulet, K. Hattori, K. Konno, A. Tanaka, R. Bosmans, M. Sawada, and H. Yazawa. Fresnel lens sidewall design for imaging optics. *Journal of the European Optical Society-Rapid publications*, 10, 2015.

[14] J.-Y. Hong, C.-K. Lee, S. Lee, B. Lee, D. Yoo, C. Jang, J. Kim, J. Jeong, and B. Lee. See-through optical combiner for augmented reality head-mounted display: index-matched anisotropic crystal lens. *Scientific reports*, 7(1):1–11, 2017.

[15] H. Huang and H. Hua. An integral-imaging-based head-mounted light field display using a tunable lens and aperture array. *Journal of the Society for Information Display*, 25(3):200–207, 2017.

[16] C. Jang, K. Bang, S. Moon, J. Kim, S. Lee, and B. Lee. Retinal 3d: Augmented reality near-eye display via pupil-tracked light field projection on retina. *ACM Trans. Graph.*, 36(6), Nov. 2017.

[17] D. Karl, K. Soderquest, M. Farhi, A. Grant, D. P. Krohn, B. Murphy, J. Schneiderman, and B. Straughan. 2019 augmented and virtual reality survey report, 2019.

[18] J. Kim, Y. Jeong, M. Stengel, K. Akşit, R. Albert, B. Boudaoud, T. Greer, J. Kim, W. Lopes, Z. Majercik, et al. Foveated ar: dynamically-foveated augmented reality display. *ACM Transactions on Graphics (TOG)*, 38(4):1–15, 2019.

[19] G. A. Koulieris, K. Akşit, M. Stengel, R. K. Mantiuk, K. Mania, and C. Richardt. Near-eye display and tracking technologies for virtual and augmented reality. In *Computer Graphics Forum*, volume 38, pages 493–519. Wiley Online Library, 2019.

[20] B. C. Kress and W. J. Cummings. 11-1: Invited paper: Towards the ultimate mixed reality experience: Hololens display architecture choices. In *SID Symposium Digest of Technical Papers*, volume 48, pages 127–131. Wiley Online Library, 2017.

[21] D. Lanman and D. Luebke. Near-eye light field displays. *ACM Trans. Graph.*, 32(6), Nov. 2013.

[22] D. Lanman and D. Luebke. Hybrid optics for near-eye displays, Jan. 30 2018. US Patent 9,880,325.

[23] T. Levola. Diffractive optics for virtual reality displays. *Journal of the Society for Information Display*, 14(5):467–475, 2006.

[24] A. Maimone, D. Lanman, K. Rathinavel, K. Keller, D. Luebke, and H. Fuchs. Pinlight displays: Wide field of view augmented reality eyeglasses using defocused point light sources. In *ACM SIGGRAPH 2014 Emerging Technologies*, SIGGRAPH '14, New York, NY, USA, 2014. Association for Computing Machinery.

[25] A. Maimone and J. Wang. Holographic optics for thin and lightweight virtual reality. *ACM Transactions on Graphics (TOG)*, 39(4):67–1, 2020.

[26] K. Masaoka, Y. Nishida, M. Sugawara, E. Nakasu, and Y. Nojiri. Sensation of realness from high-resolution images of real objects. *IEEE transactions on broadcasting*, 59(1):72–83, 2013.

[27] S. Moon, C.-K. Lee, S.-W. Nam, C. Jang, G.-Y. Lee, W. Seo, G. Sung, H.-S. Lee, and B. Lee. Augmented reality near-eye display using pancharatnam-berry phase lenses. *Scientific reports*, 9(1):1–10, 2019.

[28] S. Moon, S.-W. Nam, Y. Jeong, C.-K. Lee, H.-S. Lee, and B. Lee. Compact augmented reality combiner using pancharatnam-berry phase lens. *IEEE Photonics Technology Letters*, 32(5):235–238, 2020.

[29] B. Narasimhan. Ultra-compact pancake optics based on thineyes super-resolution technology for virtual reality headsets. page 134, 05 2018.

[30] H. S. Park, R. Hoskinson, H. Abdollahi, and B. Stoeber. Compact near-eye display system using a superlens-based microlens array magnifier. *Optics Express*, 23(24):30618–30633, 2015.

[31] K. Pfeiffer, L. Ghazaryan, U. Schulz, and A. Szeghalmi. Wide-angle broadband antireflection coatings prepared by atomic layer deposition. *ACS Applied Materials & Interfaces*, 11(24):21887–21894, 2019.

[32] J.-A. Piao, G. Li, M.-L. Piao, and N. Kim. Full color holographic optical element fabrication for waveguide-type head mounted display using photopolymer. *J. Opt. Soc. Korea*, 17(3):242–248, Jun 2013.

[33] J. Ratcliff, A. Supikov, S. Alfaro, and R. Azuma. Thinvr: Heterogeneous microlens arrays for compact, 180 degree fov vr near-eye displays. *IEEE Transactions on Visualization and Computer Graphics*, 26(5):1981–1990, 2020.

[34] K. Ratnam, R. Konrad, D. Lanman, and M. Zannoli. Retinal image quality in near-eye pupil-steered systems. *Optics Express*, 27(26):38289–38311, 2019.

[35] J. P. Rolland, A. Yoshida, L. D. Davis, and J. H. Reif. High-resolution inset head-mounted display. *Applied optics*, 37(19):4183–4193, 1998.

[36] R. Shi, J. Liu, H. Zhao, Z. Wu, Y. Liu, Y. Hu, Y. Chen, J. Xie, and Y. Wang. Chromatic dispersion correction in planar waveguide using one-layer volume holograms based on three-step exposure. *Appl. Opt.*, 51(20):4703–4708, Jul 2012.

[37] G. Tan, Y.-H. Lee, T. Zhan, J. Yang, S. Liu, D. Zhao, and S.-T. Wu. Foveated imaging for near-eye displays. *Optics express*, 26(19):25076–25085, 2018.

[38] H. Urey and K. D. Powell. Microlens-array-based exit-pupil expander for full-color displays. *Applied optics*, 44(23):4930–4936, 2005.

[39] G. Vallerotto, S. Askins, M. Victoria, I. Antón, and G. Sala. A novel achromatic fresnel lens for high concentrating photovoltaic systems. In *AIP Conference Proceedings*, volume 1766, page 050007. AIP Publishing LLC, 2016.

[40] G. Wetzstein, D. R. Lanman, M. W. Hirsch, and R. Raskar. Tensor displays: compressive light field synthesis using multilayer displays with directional backlighting. 2012.

[41] B. Wheelwright, J. Gollier, and M. Geng. Hybrid fresnel lens with reduced artifacts, Nov. 20 2018. US Patent 10,133,076.

[42] T. L. Wong, Z. Yun, G. Ambur, and J. Etter. Folded optics with birefringent reflective polarizers. In B. C. Kress and P. Schelkens, editors, *Digital Optical Technologies 2017*, volume 10335, pages 84 – 90. International Society for Optics and Photonics, SPIE, 2017.

[43] J.-Y. Wu, P.-Y. Chou, K.-E. Peng, Y.-P. Huang, H.-H. Lo, C.-C. Chang, and F.-M. Chuang. Resolution enhanced light field near eye display using e-shifting method with birefringent plate. *Journal of the Society for Information Display*, 26(5):269–279, 2018.

[44] Y. Yamaguchi and Y. Takaki. See-through integral imaging display with background occlusion capability. *Appl. Opt.*, 55(3):A144–A149, Jan 2016.

[45] C. Yao, D. Cheng, and Y. Wang. Design and stray light analysis of a lenslet-array-based see-through light-field near-eye display. In *Digital Optics for Immersive Displays*, volume 10676, page 106761A. International Society for Optics and Photonics, 2018.

[46] T. Zhan, J. Zou, J. Xiong, H. Chen, S. Liu, Y. Dong, and S.-T. Wu. Planar optics enables chromatic aberration correction in immersive near-eye displays. In *Optical Architectures for Displays and Sensing in Augmented, Virtual, and Mixed Reality (AR, VR, MR)*, volume 11310, page 1131003. International Society for Optics and Photonics, 2020.

[47] N. Zhang, J. Liu, J. Han, X. Li, F. Yang, X. Wang, B. Hu, and Y. Wang. Improved holographic waveguide display system. *Applied Optics*, 54(12):3645–3649, 2015.